ORGANOMETALLICS

Article

pubs.acs.org/Organometallics

Ligand Perturbations on Fluorescence of Dinuclear Platinum Complexes of 5,12-Diethynyltetracene: A Spectroscopic and Computational Study

Minh-Hai Nguyen,[†] Chun-Yuen Wong,*[,‡] and John H. K. Yip*[,†]

[†]Department of Chemistry, National University of Singapore, 3 Science Drive 3, Singapore 117543

[‡]Department of Biology and Chemistry, City University of Hong Kong, Tat Chee Avenue, Kowloon, Hong Kong SAR, People's Republic of China

Supporting Information

ABSTRACT: To understand how the Pt^{II} ion perturbs the electronic structures of tetracene, 10 dinuclear $[X(Et_3P)_2Pt^{II}]_2$-5,12-diethynyltetracene complexes with different auxiliary ligands were synthesized. Interactions between the Pt^{II} ion and 5,12-diethynyltetracene were probed spectroscopically and computationally. The dinuclear $[X(Et_3P)_2Pt^{II}]_2$-5,12-diethynyltetracene complexes exhibit red-shifted absorption and fluorescence in comparison with those of 5,12-bis(triisopropylsilylethynyl)tetracene, with the neutral complexes with π-donating auxiliary ligands showing a larger red shift than the cationic complexes with π-accepting ligands. Electronic structures of the complexes and effects of the metal ions and the ligands on the electronic transitions of the complexes were investigated by TD-DFT calculations, the results of which showed that the electronic structure of the 5,12-diethynyltetracene core is perturbed by π interactions with the Pt fragments, the extent of which depends on the energies of the dπ orbitals of the Pt fragments.

INTRODUCTION

Oligoacenes, especially anthracene, tetracene, and pentacene, have played an important role in the development of low-dimensional materials, light-harvesting systems, optoelectronics, and organic electronics.[1] It has been demonstrated that functionalization can increase the stability or solubility of the oligoacenes and vary their photophysical properties and electron transfer parameters.[2] In addition, functionalization can change the solid-state packing of the oligoacenes, which is crucial for properties such as charge mobility and charge injection barrier.[1e,g,3] In most cases, oligoacenes are functionalized with p-block elements such as halogens, aryls, and alkynes.[4] On the other hand, transition metals have not been much employed in oligoacene functionalization, despite the potential for d orbitals to impart redox activity, new structural moiety, photophysics, and intermolecular interactions to the oligoacences.[5] It is believed that understanding how metals influence the photophysics of oligoacenes is important in developing metal−oligoacenes as a new class of organometallic emitters and devices. Some recent work shows that attaching platinum(II) and gold(I) to anthracene and pyrene can alter the photophysics and reactivity of the molecules.[6] Pt^{II} and Au^{I} tetracene and 5,12-diethynyltetracene complexes have been reported recently, and spectroscopic studies of the complexes showed that metalation together with alkynylation can red-shift the fluorescence energy of tetracene up to 0.53 eV.[7] Interestingly, the complex $[I(Et_3P)_2Pt^{II}]_2$-5,12-diethynyltetracene (**1**; Chart 1) shows a larger red shift of tetracene-centered

Chart 1

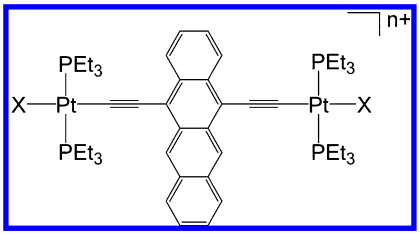

$\pi \rightarrow \pi^*$ absorption and fluorescence than the corresponding $[R_3PAu^{I}]_2$-5,12-diethynyltetracene complexes (R = CH_3, C_6H_5). We proposed that the Pt^{II} ion, being more π-donating than the Au^{I}, has stronger perturbations on the tetracenyl ring via metal-to-tetracene π-donation, mediated by the ethynyl linker. The hypothesis can be tested by a systematic variation of the electronic properties of the Pt^{II} ion. To this end, 10 homologous dinuclear $[X(Et_3P)_2Pt^{II}]_2$-5,12-diethynyltetracene complexes with different ligands X were synthesized and their spectroscopy was investigated. A spectroscopic study showed

Received: September 21, 2012
Published: March 5, 2013

   dx.doi.org/10.1021/om300904b | *Organometallics* 2013, 32, 1620−1629

that the electronic structure of the tetracenyl ring is perturbed by the metal ions. Although X is far from the central chromophore, it has a significant effect on the spectroscopy of the complexes, as it is observed that fluorescence of the neutral complexes with π-donating ligands is consistently red-shifted from those cationic complexes with π-accepting ligands. DFT calculations were carried out on model compounds to provide an explanation for the spectroscopy of the complexes.

EXPERIMENTAL SECTION

General Methods. All syntheses were carried out in a N_2 atmosphere. All the solvents used for synthesis and spectroscopic measurements were purified according to the literature procedures.[8] 5,12-Bis(triisopropylsilylethynyl)tetracene (TIPS-T)[1e] and complex **1**[7] were prepared according to the reported methods.

Physical Methods. The UV/vis absorption and emission spectra of the complexes were recorded on a Hewlett-Packard HP8452A diode array spectrophotometer and a Perkin-Elmer LS-50D fluorescence spectrophotometer, respectively. Rhodamine 640 (also known as rhodamine 101)[9] was used as a standard in measuring the emission quantum yields. Emission lifetimes were recorded on a Horiba Jobin-Yvon Fluorolog FL-1057 spectrometer. ^{1}H and ^{31}P{^{1}H} NMR spectra were recorded on a Bruker ACF 300 spectrometer. All chemical shifts are quoted relative to $SiMe_4$ (^{1}H) or H_3PO_4 (^{31}P). Elemental analyses of the complexes were carried out in the microanalysis laboratory in the Department of Chemistry at the National University of Singapore.

Synthesis of [Br(Et$_3$P)$_2$Pt^{II}]$_2$-5,12-diethynyltetracene (2). To a CH_2Cl_2 solution of **1** (50 mg, 0.036 mmol) was added AgOTf (19 mg, 0.072 mmol) with stirring at room temperature over 1 h in the absence of light. The resulting mixture was filtered under argon, and excess tetra-*n*-octylammonium bromide was added. The solution was stirred for 2 h, and the solvent was then reduced by rotary evaporation. The title compound was precipitated by the addition of excess MeOH. Yield: 22 mg, 49%. Anal. Calcd for **2** ($C_{46}H_{70}Br_2P_4Pt_2$): C, 42.60; H, 5.44. Found: C, 42.60; H, 4.96. ^{1}H NMR (300 MHz, $CDCl_3$): δ 9.34 (s, 2H, $H_{6,11}$), 8.69 (dd, J = 3.3, 6.7 Hz, 2H, $H_{1,4}$), 7.96 (dd, J = 3.0, 6.6 Hz, 2H, $H_{7,10}$), 7.42−7.37 (m, 4H, $H_{2,3,8,9}$), 2.17−2.13 (m, 24H, PCH_2CH$_3$), 1.30−1.20 (m, 36H, PCH$_2$CH_3). ^{31}P{^{1}H} NMR (121.5 MHz, $CDCl_3$): δ 13.54 (s, $^1J_{Pt-P}$ = 2360 Hz). ESI-MS: m/z 1296, [M]$^+$.

Synthesis of [Cl(Et$_3$P)$_2$Pt^{II}]$_2$-5,12-diethynyltetracene (3). The compound was prepared by following the procedure described above using tetra-*n*-butylammonium chloride. Yield: 77%. Anal. Calcd for **3** ($C_{46}H_{70}Cl_2P_4Pt_2$): C, 45.74; H, 5.84. Found: C, 45.41; H, 5.63. ^{1}H NMR (300 MHz, $CDCl_3$): δ 9.33 (s, 2H, $H_{6,11}$), 8.68 (dd, J = 3.1, 6.7 Hz, 2H, $H_{1,4}$), 7.96 (dd, J = 3.0, 6.6 Hz, 2H, $H_{7,10}$), 7.40−7.38 (m, 4H, $H_{2,3,8,9}$), 2.11−2.07 (m, 24H, PCH_2CH$_3$), 1.32−1.21 (m, 36H, PCH$_2$CH_3). ^{31}P{^{1}H} NMR (121.5 MHz, $CDCl_3$): δ 15.96 (s, $^1J_{Pt-P}$ = 2388 Hz). ESI-MS: m/z 1208.1, [M]$^+$.

Synthesis of [C$_6$H$_5$S(Et$_3$P)$_2$Pt^{II}]$_2$-5,12-diethynyltetracene (4). To a stirred solution of **1** (44 mg, 0.032 mmol) in CH_2Cl_2 (10 mL) were added thiophenol (0.1 mL, 1 mmol) and NEt_3 (0.2 mL, 1.3 mmol). The resulting mixture was stirred for 2 h, and the solvent was then reduced by rotary evaporation. The addition of excess MeOH afforded a deep purple solid. The product was filtered and thoroughly washed with MeOH and then dried in vacuo. Yield: 27 mg, 63%. X-ray-quality crystals of **4** were obtained from CH_2Cl_2/MeOH at room temperature. Anal. Calcd for **4** ($C_{58}H_{80}P_4Pt_2S_2$): C, 51.39; H, 5.95; S, 4.73. Found: C, 51.00; H, 5.83; S, 4.67. ^{1}H NMR (300 MHz, $CDCl_3$): δ 9.39 (s, 2H, $H_{6,11}$), 8.74 (dd, J = 3.4, 6.9 Hz, 2H, $H_{1,4}$), 8.00 (dd, J = 3.1, 6.6 Hz, 2H, $H_{7,10}$), 7.61 (d, J = 8.2 Hz, 4H, o-C_6H_5), 7.43−7.38 (m, 4H, $H_{2,3,8,9}$), 7.11−7.06 (m, 4H, m-C_6H_5), 6.93 (t, J = 6.6 Hz, 2H, p-C_6H_5), 2.09−2.03 (m, 24H, PCH_2CH$_3$), 1.27−1.16 (m, 36H, PCH$_2$CH_3). ^{31}P{^{1}H} NMR (121.5 MHz, $CDCl_3$): δ 13.29 (s, $^1J_{Pt-P}$ = 2412 Hz). ESI-MS: m/z 1354.5, [M]$^+$.

Synthesis of [C$_6$H$_5$Se(Et$_3$P)$_2$Pt^{II}]$_2$-5,12-diethynyltetracene (5). The compound was prepared by following the procedure for **4** using benzeneselenol. Yield: 67%. X-ray-quality crystals of **5** were obtained from THF/MeOH at room temperature. Anal. Calcd for **5** ($C_{58}H_{80}P_4Pt_2Se_2$): C, 48.07; H, 5.56. Found: C, 48.08; H, 5.71. ^{1}H NMR (300 MHz, $CDCl_3$): δ 9.40 (s, 2H, $H_{6,11}$), 8.74 (dd, J = 3.3, 6.7 Hz, 2H, $H_{1,4}$), 8.00 (dd, J = 3.1, 6.6 Hz, 2H, $H_{7,10}$), 7.74 (d, J = 5.6 Hz, 4H, o-C_6H_5), 7.44−7.38 (m, 4H, $H_{2,3,8,9}$), 7.07−7.05 (m, 6H, m,p-C_6H_5), 2.14−2.09 (m, 24H, PCH_2CH$_3$), 1.26−1.16 (m, 36H, PCH$_2$CH_3). ^{31}P{^{1}H} NMR (121.5 MHz, $CDCl_3$): δ 10.80 (s, $^1J_{Pt-P}$ = 2392 Hz). ESI-MS: m/z 1450.0, [M]$^+$.

Synthesis of [C$_6$H$_5$C}C(Et$_3$P)$_2$Pt^{II}]$_2$-5,12-diethynyltetracene (6). To a stirred solution of **1** (77 mg, 0.055 mmol) in THF (10 mL) were added CuI (5 mg), diethylamine (5 mL), and phenylacetylene (0.12 mL, 1 mmol). The resulting mixture was stirred overnight, and all the solvents were removed in vacuo. The solid residue was extracted with CH_2Cl_2, and the title compound was afforded by the addition of excess MeOH. Yield: 37 mg, 50%. X-ray-quality crystals of **6** were obtained from CH_2Cl_2/MeOH at room temperature. Anal. Calcd for **6** ($C_{62}H_{80}P_4Pt_2$): C, 55.60; H, 6.02. Found: C, 55.31; H, 5.85. ^{1}H NMR (300 MHz, $CDCl_3$): δ 9.39 (s, 2H, $H_{6,11}$), 8.74 (dd, J = 3.4, 6.9 Hz, 2H, $H_{1,4}$), 7.96 (dd, J = 3.0, 6.4 Hz, 2H, $H_{7,10}$), 7.39−7.33 (m, 8H, $H_{2,3,8,9}$ and o-C_6H_5), 7.24−7.22 (m, 4H, m-C_6H_5), 7.14 (t, J = 7.2 Hz, 2H, p-C_6H_5), 2.26−2.20 (m, 24H, PCH_2CH$_3$), 1.35−1.24 (m, 36H, PCH$_2$CH_3). ^{31}P{^{1}H} NMR (121.5 MHz, $CDCl_3$): δ 12.27 (s, $^1J_{Pt-P}$ = 2375 Hz). FAB-MS: m/z 1338.6, [M]$^+$.

Synthesis of [Ph$_3$P(Et$_3$P)$_2$Pt^{II}]$_2$-5,12-diethynyltetracene (7). The compound was prepared by following the procedure for **2**, except that Ph_3P was used instead of tetra-*n*-octylammonium bromide and the titled compound was precipitated by the addition of excess Et_2O. Yield: 85%. Slow diffusion of Et_2O into a CH_2Cl_2 solution at room temperature afforded red crystals suitable for X-ray crystallography study. Anal. Calcd for **7** ($C_{84}H_{100}F_6O_6P_6Pt_2S_2$): C, 51.48; H, 5.14; S, 3.27. Found: C, 51.16; H, 5.03; S, 3.12. ^{1}H NMR (300 MHz, $CDCl_3$): δ 9.27 (s, 2H, $H_{6,11}$), 8.62 (dd, J = 3.2, 6.7 Hz, 2H, $H_{1,4}$), 8.06 (dd, J = 3.4, 6.5 Hz, 2H, $H_{7,10}$), 7.91−7.46 (m, 34H, $H_{2,3,8,9}$ and C_6H_5), 1.71−1.67 (m, 24H, PCH_2CH$_3$), 1.17−1.07 (m, 36H, PCH$_2$CH_3). ^{31}P{^{1}H} NMR (121.5 MHz, $CDCl_3$): δ 12.91 (t, $^1J_{Pt-P}$ = 2561 Hz, $^2J_{P-P}$ = 22 Hz, PPh$_3$), 8.62 (d, $^1J_{Pt-P}$ = 2173 Hz, $^2J_{P-P}$ = 22 Hz, PEt$_3$) . ESI-MS: m/z 830.7, [M − 2OTf]$^{2+}$.

Synthesis of [(Et$_3$P)$_3$Pt^{II}]$_2$-5,12-diethynyltetracene (8). The compound was prepared following the procedure for **7**, except that Et_3P was used instead of Ph_3P. Yield: 75%. Crystals of **8** were grown by slow diffusion of Et_2O into an acetone solution. Anal. Calcd for **8** ($C_{60}H_{100}F_6O_6P_6Pt_2S_2$): C, 43.11; H, 6.03; S, 3.84. Found: C, 43.22; H, 5.86; S, 3.64. ^{1}H NMR (300 MHz, $CDCl_3$): δ 9.18 (s, 2H, $H_{6,11}$), 8.52 (dd, J = 3.3, 6.7 Hz, 2H, $H_{1,4}$), 7.93 (dd, J = 3.4, 6.6 Hz, 2H, $H_{7,10}$), 7.49−7.47 (m, 4H, $H_{2,3,8,9}$), 2.29−2.17 (m, 36H, PCH_2CH$_3$), 1.36−1.24 (m, 54H, PCH$_2$CH_3). ^{31}P{^{1}H} NMR (121.5 MHz, $CDCl_3$): δ 12.60 (d, $^1J_{Pt-P}$ = 2223 Hz, $^2J_{P-P}$ = 24 Hz, P_{cis}), 6.38 (t, $^1J_{Pt-P}$ = 2403 Hz, $^2J_{P-P}$ = 24 Hz, P_{trans}) . ESI-MS: m/z 686.2, [M − 2OTf]$^{2+}$.

Synthesis of [C$_5$H$_5$N(Et$_3$P)$_2$Pt^{II}]$_2$-5,12-diethynyltetracene (9). The compound was prepared following the procedure for **7**, except that pyridine was used instead of Ph_3P. Yield: 63%. Slow diffusion of of Et_2O into a CH_2Cl_2 solution at room temperature afforded red crystals suitable for an X-ray crystallography study. Anal. Calcd for **9** ($C_{58}H_{80}F_6N_2O_6P_4Pt_2S_2$): C, 43.72; H, 5.06; N, 1.76; S, 4.02. Found: C, 43.32; H, 5.22; N, 1.69; S, 4.01. ^{1}H NMR (300 MHz, $CDCl_3$): δ 9.21 (s, 2H, $H_{6,11}$), 8,74 (d, J = 4.9 Hz, 4H, o-C_5H_5N), 8.56 (dd, J = 3.3, 6.6 Hz, 2H, $H_{1,4}$), 8.07 (t, J = 7.9 Hz, 2H, p-C_5H_5N), 7.96 (dd, J = 3.4, 6.7 Hz, 2H, $H_{7,10}$), 7.81−7.76 (m, 4H, m-C_5H_5N), 7.47−7.42 (m, 4H, $H_{2,3,8,9}$), 1.80−1.75 (m, 24H, PCH_2CH$_3$), 1.27−1.16 (m, 36H, PCH$_2$CH_3). ^{31}P{^{1}H} NMR (121.5 MHz, $CDCl_3$): δ 16.50 (s, $^1J_{Pt-P}$ = 2320 Hz). ESI-MS: m/z 647.1, [M − 2OTf]$^{2+}$.

Synthesis of [C$_6$H$_3$(CH$_3$)$_2$N}C(Et$_3$P)$_2$Pt^{II}]$_2$-5,12-diethynyltetracene (10). To a suspension of **1** (40 mg, 0.029 mmol) in acetonitrile (5 mL) was added 2,6-xylyl isocyanide (10 mg, 0.076 mmol). When it was stirred for 1 h, the suspension turned into a clear orange-red solution. The addition of excess NaOTf (100 mg) followed by Et_2O afforded the title product, which was collected and dried. Yield: 26 mg, 53%. Anal. Calcd for **10** ($C_{66}H_{88}F_6N_2O_6P_4Pt_2S_2$): C, 46.70; H, 5.22; N, 1.65; S, 3.78. Found: C, 46.60; H, 5.02; N, 1.61; S, 3.70. ^{1}H NMR (300 MHz, $CDCl_3$): δ 9.19 (s, 2H, $H_{6,11}$), 8.54 (dd, J = 3.3, 6.9 Hz,

dx.doi.org/10.1021/om300904b | Organometallics 2013, 32, 1620−1629

Table 1. X-ray Crystal Data for 4−6, 7·2CH_2Cl_2, 8·0.5C_3H_6O·H_2O, and 9·2CH_2Cl_2

	4	5	6	7·2CH_2Cl_2	8·0.5C_3H_6O·H_2O	9·2CH_2Cl_2
empirical formula	$C_{58}H_{80}P_4Pt_2S_2$	$C_{58}H_{80}P_4Pt_2Se_2$	$C_{62}H_{80}P_4Pt_2$	$C_{86}H_{104}Cl_4F_6O_6P_6Pt_2S_2$	$C_{61.5}H_{105}F_6O_{7.5}P_6Pt_2S_2$	$C_{60}H_{84}Cl_4F_6N_2O_6P_4Pt_2S_2$
formula wt	1355.40	1449.20	1339.32	2129.61	1716.56	1763.27
cryst syst	monoclinic	monoclinic	triclinic	triclinic	monoclinic	monoclinic
space group	$P2_1/c$	$P2_1/c$	$P\bar{1}$	$P\bar{1}$	$P2_1/n$	$C2/c$
unit cell dimens						
a (Å)	9.2161(11)	8.9050(8)	9.5196(48)	9.4901(4)	22.9582(10)	9.2429(8)
b (Å)	25.684(3)	11.5177(11)	17.2407(8)	11.5318(5)	10.8973(5)	20.0203(17)
c (Å)	12.9507(15)	27.949(3)	18.7566(8)	20.5678(9)	29.5076(13)	37.838(3)
α (deg)	90	90	71.520(1)	81.069(1)	90	90
β (deg)	109.035	93.569	80.678(1)	89.872(1)	91.500(1)	95.066(2)
γ (deg)	90	90	81.328(1)	80.764(1)	90	90
V (Å^3)	2897.9(6)	2861.1(5)	2864.8(2)	2194.19(16)	7379.8(6)	6794.5(10)
Z	2	2	2	1	4	4
calcd density (g cm^{-3})	1.553	1.682	1.553	1.612	1.545	1.679
abs coeff (mm^{-1})	5.040	6.304	5.027	3.527	4.035	4.376
F(000)	1352	1424	1336	1068	3456	3504
cryst size (mm^3)	0.3 × 0.18 × 0.14	0.30 × 0.14 × 0.04	0.40 × 0.16 × 0.08	0.56 × 0.30 × 0.28	0.40 × 0.30 × 0.02	0.78 × 0.16 × 0.10
θ range for data collection (deg)	1.59−25.00	1.91−25.00	1.15−25.00	1.00−27.50	1.14−25.00	2.11−27.50
index ranges	$-10 \le h \le 10$	$-10 \le h \le 10$	$-11 \le h \le 11$	$-12 \le h \le 12$	$-27 \le h \le 27$	$-11 \le h \le 11$
	$-30 \le k \le 25$	$-13 \le k \le 13$	$-20 \le k \le 20$	$-14 \le k \le 14$	$-8 \le k \le 12$	$-24 \le k \le 26$
	$-15 \le l \le 14$	$-15 \le l \le 14$	$-22 \le l \le 22$	$-26 \le l \le 26$	$-34 \le l \le 35$	$-41 \le l \le 49$
no. of rflns collected	16478	16058	31021	29069	41224	24544
no. of indep rflns	5102 (R(int) = 0.0872)	5042 (R(int) = 0.0676)	10103 (R(int) = 0.0330)	10053 (R(int) = 0.0379)	12968 (R(int) = 0.0502)	8006 (R(int) = 0.0317)
max, min transmission	0.5389, 0.3132	0.7866, 0.2536	0.6892, 0.2384	0.4384, 0.2427	0.9236, 0.2952	0.6687, 0.1315
no. of data/restraints/params	5102/381/507	5042/286/432	10103/0/625	10053/41/556	12968/548/923	8006/0/394
goodness of fit (GOF)	1.126	1.225	1.069	1.154	1.053	1.245
final R indices ($I > 2\sigma(I)$)	R1 = 0.0844, wR2 = 0.1687	R1 = 0.0863, wR2 = 0.1717	R1 = 0.0357, wR2 = 0.0879	R1 = 0.0395, wR2 = 0.0974	R1 = 0.0572, wR2 = 0.1438	R1 = 0.0416, wR2 = 0.0931
largest diff peak, hole (e Å^{-3})	1.944, −1.307	1.432, −2.069	3.947, −1.176	1.841, −1.358	3.350, −2.394	1.886, −2.378

2H, $H_{1,4}$), 7.98 (dd, J = 3.3, 6.6 Hz, 2H, $H_{7,10}$), 7.53−7.26 (m, 10H, $H_{2,3,8,9}$ and C_6H_3), 2.56 (s, 12H, CH_3), 2.33−2.28 (m, 24H, PCH_2CH_3), 1.40−1.29 (m, 36H, PCH_2CH_3). $^{31}P\{^1H\}$ NMR (121.5 MHz, $CDCl_3$): δ 17.31 (s, $^1J_{Pt-P}$ = 2068 Hz). ESI-MS: m/z 699.3, $[M - 2OTf]^{2+}$.

X-ray Crystallography. The diffraction experiments were carried out on a Bruker AXS SMART CCD three-circle diffractometer with a sealed tube at 223 K using graphite-monochromated Mo Kα radiation (λ = 0.71073 Å). The software used were SMART[10] for collecting frames of data, indexing reflections, and determination of lattice parameters, SAINT[10a] for integration of intensity of reflections and scaling, SADABS[10b] for multiscan absorption correction, and SHELXTL[10c] for space group determination, structure solution, and least-squares refinements on $|F|^2$. Anisotropic thermal parameters were refined for the rest of the non-hydrogen atoms. The hydrogen atoms were included in all refinements as riding atoms in geometrically correct positions. The molecule of **7** is equally disordered over two positions which are related by a C_2 rotation around the substituted ring of the tetracenyl ring. The X-ray crystal data are summarized in Table 1.

Computation Methodology. DFT and TD-DFT calculations were performed on $\{[X(PMe_3)_2Pt]_2$-5,12-diethynyltetracene$\}^{n+}$ (X = $^-$SPh (**4′**), $^-$SePh (**5′**), $^-$C≡CPh (**6′**), n = 0; X = PMe_3 (**8′**), pyridine (**9′**), C≡NPh (**10′**), n = 2), which were used as models for the platinum complexes studied in this work. PMe_3 was used instead of PEt_3 in the models in order to reduce computational effort. 5,12-Bis(trimethylsilylethynyl)tetracene and 5,12-diethynyltetracene were also computed for comparisons. Their electronic ground states were optimized without symmetry imposed using Becke's three-parameter hybrid functional[11] with the Lee−Yang−Parr correlation functional[12] (B3LYP). Frequency calculations were also performed on all the optimized structures. As no imaginary vibrational frequencies were encountered, the optimized stationary points were confirmed to be local minima. Detailed optimized structural data are summarized in the Supporting Information (Tables S1−S7).

In each TD-DFT calculation, the direction along the Pt−C(acetylide) is defined to coincide with the z axis of the coordinate system and the Pt−P bond in the x direction. Stuttgart small-core relativistic effective core potentials were employed for Pt atoms with their accompanying basis sets.[13] In the geometry optimization calculations, the 6-31G basis set was employed for C and H atoms[14] and the 6-311G basis set for N, P, S, and Se atoms.[15] The vertical transition energies (the first 160 excited states) for the model complexes were computed at their respective gas-phase-optimized ground-state geometries using the TD-B3LYP method. The 6-31G* basis set was employed for C and H atoms in the TD-DFT calculations in order to enhance the accuracy of calculations. Tight SCF convergence (10^{-8} au) was used for all calculations. All the DFT and TD-DFT calculations were performed using the Gaussian 03 program package (revision D.01).[16]

RESULTS AND DISCUSSION

Complex **1** was synthesized from Cu(I)/amine coupling[17] between *trans*-$[Pt(PEt_3)_2I_2]$ and 5,12-diethynyltetracene, which was produced from desilylation of 5,12-bis(triisopropylsilylethynyl)tetracene (TIPS-T) followed by deprotonation. Except for **6**, which was prepared by Cu(I)/amine coupling of **1** and phenylacetylide, all complexes were synthesized from **1** by substitution of its iodides with X. The

dx.doi.org/10.1021/om300904b | Organometallics 2013, 32, 1620−1629

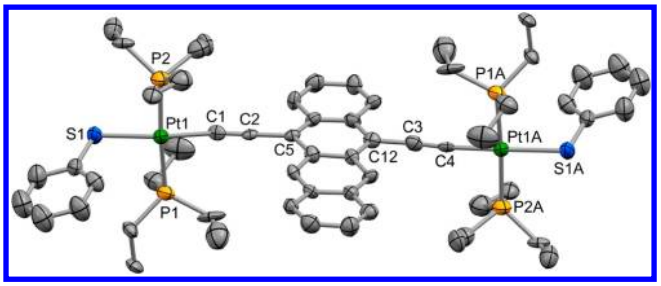

Figure 1. ORTEP plot of **4** (thermal ellipsoids drawn at the 30% probability level). Disordered parts of tetracene and ethyl groups are not shown for clarity. Color scheme: Pt, green; P, orange; C, gray; S, blue.

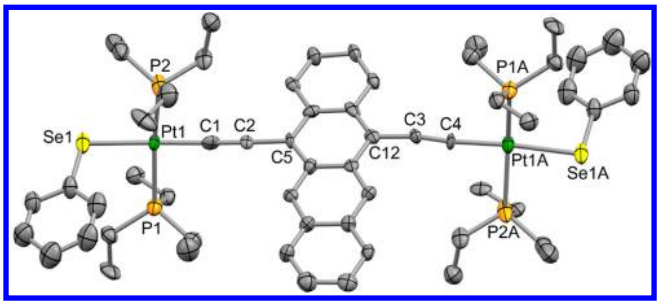

Figure 2. ORTEP plot of **5** (thermal ellipsoids drawn at the 30% probability level). Disordered parts of tetracene and ethyl groups are not shown for clarity. Color scheme: Pt, green; P, orange; C, gray; Se, yellow.

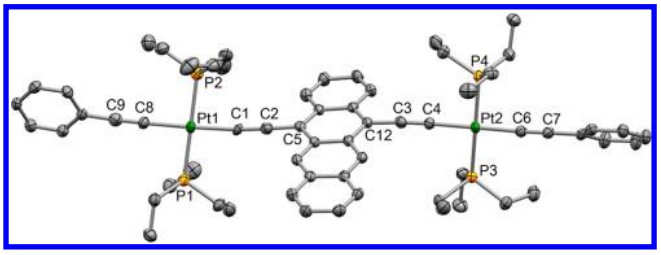

Figure 3. ORTEP plot of **6** (thermal ellipsoids drawn at the 50% probability level). Color scheme: Pt, green; P, orange; C, gray.

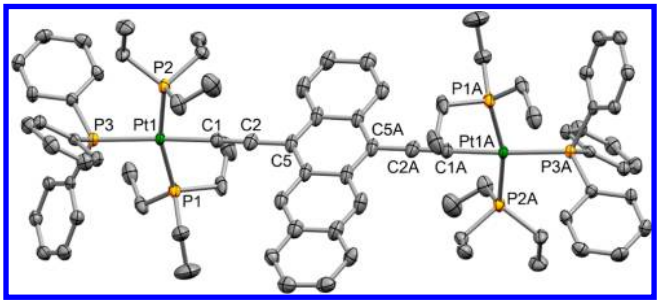

Figure 4. ORTEP plot of **7**·2CH_2Cl_2 (thermal ellipsoids drawn at the 50% probability level). H atoms, the anions, solvent molecules, and the disordered part of tetracene are not shown for clarity. Color scheme: Pt, green; P, orange; C, gray.

cationic **7**−**10** were isolated as triflate salts. Crystal structures of **4**−**9** are shown in Figures 1−6, respectively, and the selected structural parameters are given in Tables 2 and 3. The tetracenyl rings in **4** and **5** are severely disordered, resulting in relatively less accurate Pt−C bond distances and X−Pt−C and P−Pt−C bond angles. All complexes show similar 5,12-

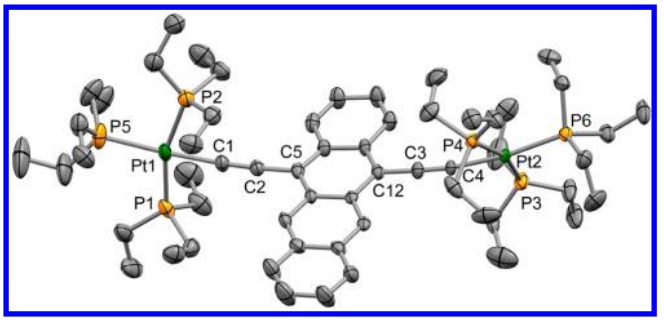

Figure 5. ORTEP plot of **8**·0.5C_3H_6O·H_2O (thermal ellipsoids drawn at the 30% probability level). The anions and solvent molecules are not shown for clarity. Color scheme: Pt, green; P, orange; C, gray.

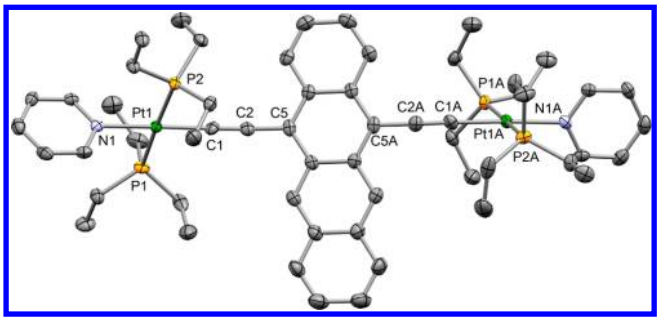

Figure 6. ORTEP plot of **9**·2CH_2Cl_2 (thermal ellipsoids drawn at the 50% probability level). The anions and solvent molecules are not shown for clarity. Color scheme: Pt, green; P, orange; C, gray; N, light blue.

Table 2. Selected Bond Lengths (Å) and Angles (deg) of 4−6

4			
Pt(1)−C(1)	1.99(3)	Pt(1)−P(1)	2.305(5)
Pt(1)−S(1)	2.350(4)	Pt(1)−P(2)	2.283(5)
Pt(1A)-C(4)	1.97(3)		
C(1)−Pt(1)−S(1)	168.8(10)	S(1)−Pt(1)−P(2)	91.2(2)
P(1)−Pt(1)−P(2)	174.84(19)	C(1)−C(2)−C(5)	172(4)
C(1)−Pt(1)−P(2)	88.8(11)		
5			
Pt(1)−C(1)	1.93(3)	Pt(1)−P(1)	2.383(6)
Pt(1)−Se(1)	2.473(5)	Pt(1)−P(2)	2.248(6)
C(1)−Pt(1)−Se(1)	174.7(9)	Se(1)−Pt(1)−P(2)	89.8(2)
P(1)−Pt(1)−P(2)	171.5(3)	C(1)−C(2)−C(5)	178(3)
C(1)−Pt(1)−P(2)	88.4(11)		
6			
Pt(1)−C(1)	2.000(5)	Pt(1)−P(1)	2.3004(14)
Pt(1)−C(7)	2.001(5)	Pt(1)−P(2)	2.3019(15)
C(1)−Pt(1)−C(7)	177.8(2)	C(7)−Pt(1)−P(1)	87.43(16)
P(1)−Pt(1)−P(2)	178.46(5)	C(1)−Pt(1)−P(1)	94.70(15)
C(1)−Pt(1)−P(2)	85.59(16)	C(1)−C(2)−C(5)	178.4(6)

diethynyltetracene cores with two Pt ions coordinated to the acetylides. The Pt^{II} ions show distorted-square-planar geometry with typical Pt−C(acetylide) and Pt−P(Et_3) bond distances.[18] The Pt−C(acetylide) bond distance is not affected by the different ligand field strengths of the opposite ligands. For instance, **6**−**8** have very similar Pt−C(acetylide) bond distances, despite the different σ-donating and π-accepting strengths of PhC≡C$^-$, PPh_3, and PEt_3. Bond distances between the metal and other auxiliary ligands are normal.[19]

dx.doi.org/10.1021/om300904b | *Organometallics* 2013, 32, 1620−1629

Table 3. Selected Bond Lengths (Å) and Angles (deg) of $7\cdot 2CH_2Cl_2$, $8\cdot 0.5C_3H_6O\cdot H_2O$, and $9\cdot 2CH_2Cl_2$

$7\cdot 2CH_2Cl_2$			
Pt(1)−C(1)	1.987(5)	Pt(1)−P(2)	2.3450(12)
Pt(1)−P(1)	2.3347(13)	Pt(1)−P(3)	2.3170(11)
C(1)−Pt(1)−P(3)	171.83(15)	P(3)−Pt(1)−P(2)	95.54(4)
P(1)−Pt(1)−P(2)	164.19(4)	C(1)−C(2)−C(5)	178.3(6)
C(1)−Pt(1)−P(2)	81.53(14)		
$8\cdot 0.5C_3H_6O\cdot H_2O$			
Pt(1)−C(1)	1.999(9)	Pt(1)−P(1)	2.338(3)
Pt(1)−P(2)	2.360(3)	Pt(1)−P(5)	2.319(3)
C(1)−Pt(1)−P(5)	176.3(3)	P(5)−Pt(1)−P(2)	96.36(13)
P(1)−Pt(1)−P(2)	160.97(10)	C(1)−C(2)−C(5)	174.0(10)
C(1)−Pt(1)−P(2)	79.9(3)		
$9\cdot 2CH_2Cl_2$.			
Pt(1)−C(1)	1.951(5)	Pt(1)−P(2)	2.3170(12)
Pt(1)−P(1)	2.3172(12)	Pt(1)−N(1)	2.086(4)
C(1)−Pt(1)−N(1)	177.30(19)	N(1)−Pt(1)−P(1)	91.39(11)
P(1)−Pt(1)−P(2)	175.33(5)	C(1)−C(2)−C(5)	175.1(5)
C(1)−Pt(1)−P(1)	90.10(15)		

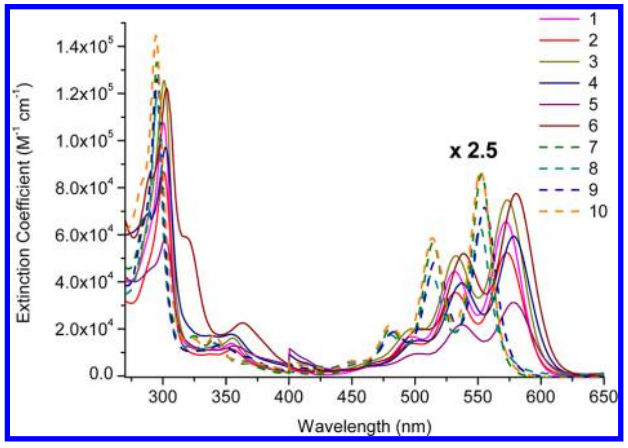

Figure 7. Absorption spectra of **1**−**6** (solid lines) and **7**−**10** (dashed lines) in CH_2Cl_2 at room temperature. For the sake of clarity, the visible absorption bands (400−650 nm) are magnified by 2.5 times.

The C≡C−C(tetracenyl) linkages are close to linear. The tetracenyl ring is essentially planar. Dihedral angles between the coordination planes of the Pt ions and the tetracenyl rings ranges from 64.02 to 87.85°, probably due to steric repulsion between the bulky PEt_3 and the tetracenyl ring. The two coordination planes in **7** are parallel but are separated by dihedral angles of 7.26, 7.88, 13.92, 38.61, and 53.17° in **4**−**6**, **8**, and **9**, respectively. There is no stacking of the tetracenyl rings in the crystals.

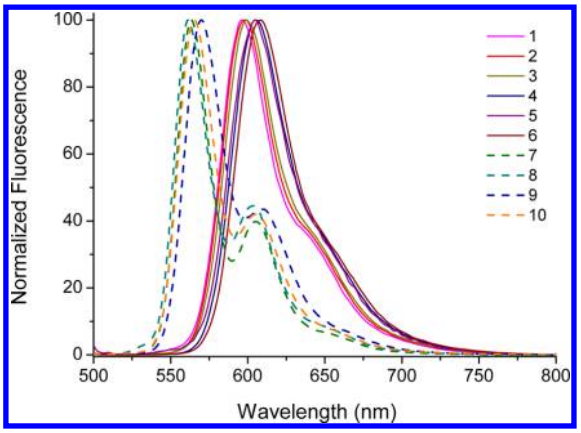

Figure 8. Emission spectra of **1**−**6** (solid lines) and **7**−**10** (dashed lines) in CH_2Cl_2 at room temperature. The excitation wavelength is 490 nm.

Absorption and Fluorescence. UV−vis absorption spectra of **1**−**10** are shown in Figure 7, and the spectral data are given in Table 4. In general, the spectra are similar and resemble those of substituted tetracenes such as 5,12-bis(triisopropylsilylethynyl)tetracene in showing three absorption bands—a very intense band at 290−300 nm (34480−33330 cm^{-1}; ε_{max} = (0.59−1.45) × 10^5 M^{-1} cm^{-1}) and two moderately intense bands at 340−360 nm (29410−27780 cm^{-1}; ε_{max} = (1.15−2.26) × 10^4 M^{-1} cm^{-1}) and 460−630 nm (21740−15870 cm^{-1}; ε_{max} = (1.25−3.50) × 10^4 M^{-1} cm^{-1}). The last band shows three vibronic peaks.

The absorption bands are due to tetracene-based $\pi \rightarrow \pi^*$ transitions perturbed by the platinated acetylene groups. On the basis of previous spectroscopic studies, the vibronic band at 460−630 nm (21740−15870 cm^{-1}) is assigned to the $S_0 \rightarrow S_1$ transition from the singlet ground state (S_0) to the lowest energy singlet excited state S_1.[7,20] It has been shown that the extent of perturbations in metalated polycyclic hydrocarbons can be gauged by red shifts of the $S_0 \rightarrow S_1$ transitions.[6a,7,21]

The transitions of the Pt complexes which are red-shifted from that of 5,12-bis(triisopropylsilylethynyl)tetracene (λ_{max} 535 nm; 18690 cm^{-1}) by 580−1450 cm^{-1}, indicating that platination increases perturbations on the electronic structure of the tetracenyl ring. The complexes can be divided into two groups based on the energies of their $S_0 \rightarrow S_1$ transitions—the neutral complexes with primarily π-donating ligands (**1**−**6**) have very similar $S_0 \rightarrow S_1$ transition energies (λ_{max} 572 − 580

Table 4. Absorption and Emission Spectroscopic Data of the Complexes

complex	$S_0 \rightarrow S_1$ transition/nm (cm^{-1}; ε, 10^4 $M^{-1}cm^{-1}$)	soln emission maximum/nm (cm^{-1})	emission lifetime τ_{fl}/ns	emission quantum yield Φ_{fl}
1	572 (17480; 2.62), 532 (18800; 1.78), 498 (20080; 0.67) (s)	596 (16780)	8.6	0.60
2	573 (17450; 2.09), 532 (18800; 1.42), 498 (20080; 0.56) (s)	599 (16690)	9.2	0.58
3	573 (17450; 2.99), 533 (18760; 2.04), 498 (20080; 0.80) (s)	599 (16690)	9.3	0.50
4	578 (17300; 2.37), 537 (18620; 1.58), 503 (19880; 0.61) (s)	605 (16530)	6.3	0.36
5	578 (17300; 1.25), 537 (18620; 0.87), 503 (19880; 0.38) (s)	605 (16530)	2.6	0.13
6	580 (17240; 3.10), 539 (18550; 2.08), 505 (19800; 0.80) (s)	608 (16450)	8.7	0.51
7	553 (18080; 3.43), 514 (19450; 2.26), 481 (20790; 0.81)	563 (17760)	2.0	0.38
8	552 (18120; 2.51), 513 (19490; 1.72), 480 (20830; 0.70)	561 (17830)	3.3	0.45
9	555 (18020; 2.85), 517 (19340; 1.96), 483 (20700; 0.75)	570 (17540)	6.5	0.81
10	552 (18120; 3.50), 514 (19450; 2.34), 481 (20790; 0.87)	565 (17700)	5.8	0.97

dx.doi.org/10.1021/om300904b | *Organometallics* 2013, 32, 1620−1629

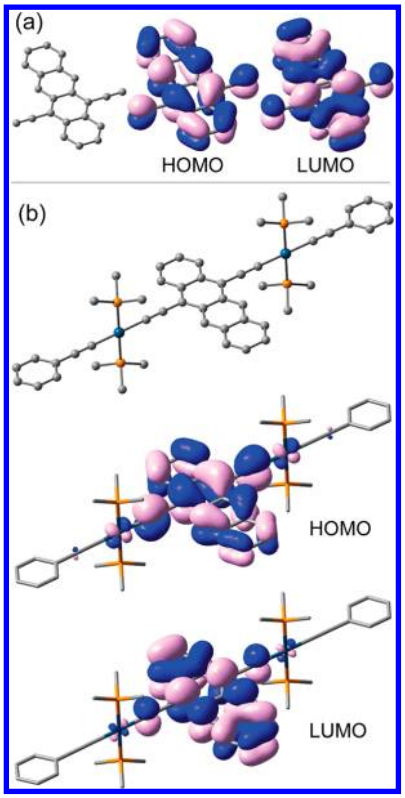

Figure 9. Optimized structures and HOMO and LUMO surfaces for (a) 5,12-diethynyltetracene (L^H) and (b) **6′** using the B3LYP functional (hydrogen atoms are omitted for clarity, surface isovalue 0.02 au).

nm; 17480−17240 cm^{-1}) which are invariably lower than the transitions (λ_{max} 552−555 nm; 18120−18020 cm^{-1}) of the cationic complexes (**7**−**10**) with primarily π-accepting ligands. The energy difference between the transitions are small (540−870 cm^{-1}) but significant, as it suggests different extents or modes of perturbation in the two classes of complexes.

The complexes are luminescent (Φ_{fl} = 0.13−0.97), with the isocyanide complex **10** being the most emissive. Like the absorption spectra, fluorescence of the complexes (Figure 8) is red-shifted from that of 5,12-bis(triisopropylsilylethynyl)-tetracene (λ_{max} 542 nm; 18450 cm^{-1}) by 620−2000 cm^{-1}. On the basis of their small Stokes shifts (290−800 cm^{-1}) and nanosecond lifetimes (2.0−9.3 ns), the emissions are assigned to metal-perturbed $S_1 \rightarrow S_0$ fluorescence. Despite of the presence of the heavy atom Pt, phosphorescence arising from triplet states of the tetracenyl core was not observed. It might be due to a low rate of intersystem crossing resulting from a large extent of π conjugation of the ligand, as suggested by Che.[22] The results are in line with previous work on Pt^{II} and Au^{I} tetracenes and 5,12-diethynyltetracenes.[7] The emission bands of the cationic complexes show vibronic shoulders more distinct than those of the neutral complexes. Analogous to the absorption spectra, the fluorescence of the neutral complexes is red-shifted from that of the cationic complexes by 770−1380 cm^{-1}.

Despite the presence of the heavy Pt atoms, no phosphorescence is observed. The fluorescence quantum yields (Φ_{fl} = 0.13−0.97) of the complexes are comparable with that of TIPS-T (Φ_{fl} = 0.79),[1e] indicating that replacing the $Si(iPr)_3$ groups with the much heavier Pt ions does not lead to a significant increase in rate of intersystem crossing from the S_1 excited state to the lowest triplet excited state T_1. This is corroborated by the long-lived S_1 excited state (τ = 2.0−9.3 ns). This apparent absence of the so-called "heavy atom effect" has been observed in other luminescent complexes containing second (e.g., Rh^{III})-[22a] or third-row transition-metal ions (e.g., Au^{I}).[22b] In a recent study, Che et al. showed that the electronic structures of the organic chromophores play a key role in controlling the rate of $S_1 \rightarrow T_1$ intersystem crossing in Au^{I} oligo(phenylethynylene) compounds.[22b] Our previous study shows that cyclometalated Pt^{II} anthracene complexes only exhibit fluorescence despite direct coordination of the metal to the aromatic ring.[6b] We argued that the absence of phosphorescence is due to the electronic structure of anthracene, which being an alternant hydrocarbon, has a large S_1-T_1 gap (11500 cm^{-1})[23] because of the strong exchange interaction between the two unpaired electrons in its extensively overlapped HOMO and LUMO. The large S_1-T_1 gap creates an unfavorable Franck−Condon barrier for the $S_1 \rightarrow T_1$ intersystem crossing. Tetracene is an alternant hydrocarbon with a large S_1-T_1 gap of 10800 cm^{-1}.[23] It is therefore possible that the apparent absence of a heavy atom effect in the present complexes is due to an unfavorable Franck−Condon barrier for the $S_1 \rightarrow T_1$ intersystem crossing.

Table 5. HOMO and LUMO Compositions of $\{[X(PMe_3)_2Pt]_2$-5,12-diethynyltetracene$\}^{n+}$

			composition/%			
complex	MO	energy/eV	$Pt[d_{xz} + p_x]$	PMe_3	5,12-diethynyltetracene	X
3′	HOMO	−4.266	8.26	4.93	86.43	0.30
	LUMO	−1.975	4.08	4.10	91.71	0.06
4′	HOMO	−4.192	9.16	4.22	84.13	2.23
	LUMO	−1.918	4.36	4.19	91.20	0.20
5′	HOMO	−4.185	8.88	4.04	83.28	3.28
	LUMO	−1.915	4.05	4.17	91.45	0.21
6′	HOMO	−4.045	7.75	4.60	86.21	1.32
	LUMO	−1.780	3.49	4.18	91.92	0.37
8′	HOMO	−8.033	4.54	5.01	88.78	1.53
	LUMO	−5.675	3.40	6.10	87.97	2.16
9′	HOMO	−7.876	4.12	3.82	91.60	0.39
	LUMO+2	−5.493	3.93	3.95	84.93	7.08
10′	HOMO	−7.988	2.91	4.00	92.48	0.59
	LUMO	−5.655	1.47	7.49	84.26	6.60

dx.doi.org/10.1021/om300904b | *Organometallics* 2013, 32, 1620−1629

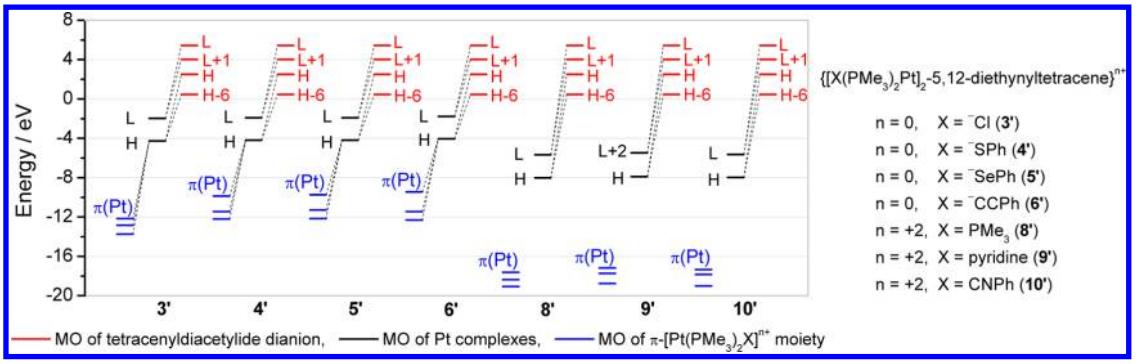

Figure 10. Orbital interaction between the $[X(PMe_3)_2Pt]^{n+}$ moieties and the 5,12-diethynyltetracene dianion in the model complexes (Interactions are counted to be effective when the percent contribution of the fragments to the model complexes >5%). H and L denote HOMO and LUMO, and π(Pt) denotes the $\{Pt[d_{xz} + p_x] + \pi(X)\}$ hybrid orbitals of the Pt fragments.

Table 6. Comparison of the Vertical Transition Energies for the Model Compounds and Corresponding Experimental Data

TD-DFT calculation			exptl data	
	excitation energy/nm (oscillator strength)	transition		λ_{max}/nm (ε_{max})
L^H	564 (0.1123)	HOMO → LUMO	L^H	*a*
L^{Si}	582 (0.2102)	HOMO → LUMO	TIPS-T	535 (3.15×10^4)
3′	606 (0.3032)	HOMO → LUMO	**3**	573 (2.99×10^4)
4′	614 (0.3648)	HOMO → LUMO	**4**	578 (2.37×10^4)
5′	616 (0.3727)	HOMO → LUMO	**5**	578 (1.25×10^4)
6′	617 (0.3945)	HOMO → LUMO	**6**	580 (3.10×10^4)
8′	588 (0.3130)	HOMO → LUMO	**8**	552 (2.51×10^4)
9′	582 (0.2547)	HOMO → LUMO+2	**9**	555 (2.85×10^4)
10′	596 (0.4001)	HOMO → LUMO	**10**	552 (3.50×10^4)

[a] 5,12-diethynyltetracene is too unstable to be isolated for spectroscopic measurements.

DFT Calculations. To understand the cause of the red shift, DFT calculations on $\{[X(PMe_3)_2Pt]_2$-5,12-diethynyltetracene$\}^{n+}$ (n = 0, X = $^-$Cl (**3′**), $^-$SPh (**4′**), $^-$SePh (**5′**), $^-$C≡CPh (**6′**); n = 2, X = PMe_3 (**8′**), pyridine (**9′**), C≡NPh (**10′**)), as models for the complexes **3**−**6**, **8**−**10** respectively, were carried out. The PEt_3 groups in the complexes are replaced with PMe_3 in the models. Also, instead of PEt_3 and 2,6-xylyl isocyanide, the auxiliary ligands in **8′** and **10′** are the electronically similar PMe_3 and phenyl isocyanide, respectively. The ground-state molecular structures of the model complexes were optimized at the DFT level (B3LYP). In order to understand the role played by the metal ions, the electronic structures of 5,12-diethynyltetracene (L^H) and 5,12-bis(trimethylsilylethynyl)tetracene (L^{Si}), which model TIPS-T, were also calculated. In each case, the directions along the Pt−C_α(5,12-diethynyltetracene) and the Pt−P bonds are defined as the z and x axes, respectively. Structural parameters of the optimized structures of the models (Supporting Information, Tables S1−S7) are in good agreement with the crystal structures of their corresponding complexes; for example, the Pt−C bond distances obtained from the X-ray crystal structures are 1.982(5) and 2.000(5) Å in **6** and 1.951(5) Å in **9** and are 2.022 and 1.975 Å in **6′** and **9′**. Figure 9 shows the optimized structures and HOMO and LUMO surfaces for L^H and **6′**. Although all the calculated molecules were optimized with no symmetry imposed, their ground-state structures have approximate C_{2v} symmetry. The HOMOs (a_2) and LUMOs (b_1) of the molecules are dominated by the π and π^* orbitals of the central 5,12-diethynyltetracenyl ring.

An exception is **9′** (n = 2, X = pyridine), for which the tetracene-based π^* orbital is LUMO+2 (LUMO and LUMO+1 are π^* orbitals of the pyridine ligands), and accordingly the HOMO → LUMO+2 transition of **9′** corresponds to the HOMO → LUMO transitions of the other complexes. The π(Pt) orbitals mix with the π and π^* orbitals of the 5,12-diethynyltetracene dianion, but their contributions to the HOMOs and LUMOs (LUMO+2 for **9′**) are small (>10% in both the HOMOs and LUMOs). For the neutral complexes with π-donating ligands (**3′**−**6′**), the Pt[d_{xz} + p_x] hybrid

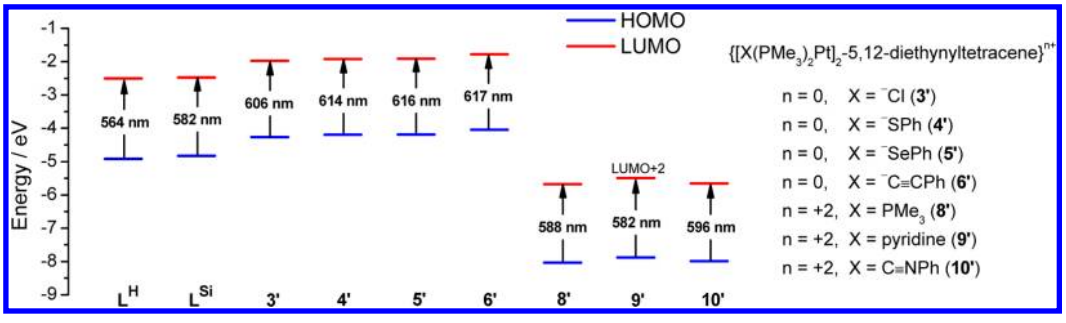

Figure 11. Energy levels of the HOMOs and LUMOs and the energies associated with the transition between the MOs for L^H, L^{Si}, and other model Pt complexes. For **9′**, LUMO+2 is depicted instead of the LUMO.

dx.doi.org/10.1021/om300904b | *Organometallics* 2013, 32, 1620−1629

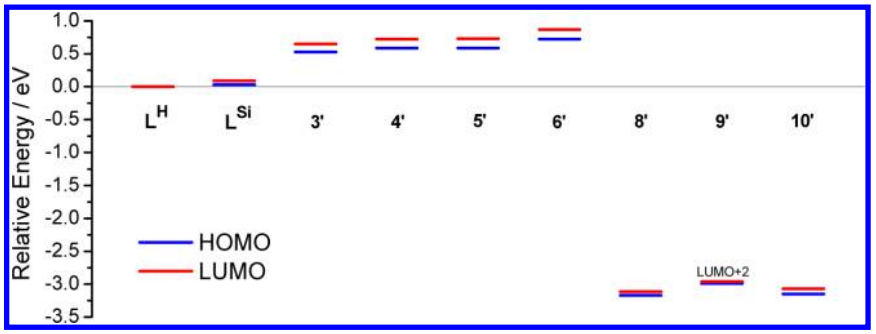

Figure 12. Energies of the HOMOs and LUMOs in the model Pt complexes relative to those in L^H.

orbitals contribute more to the HOMOs (7.75−9.16%) than to the LUMOs (3.49−4.36%); for the cationic complexes (**8′**−**10′**), the Pt[d_{xz} + p_x] hybrid orbitals have small contributions to both the HOMOs (2.91−4.54%) and LUMOs ((LUMO+2 for **9′**, 1.47−3.93%). According to the different extents of the Pt[d_{xz} + p_x] hybrid orbital contribution to the frontier orbitals, one would expect the metal perturbation in **3′**−**6′** should be stronger than in **8′**−**10′**. The compositions of the HOMOs and LUMOs (LUMO+2 for **9′**) for the model Pt complexes are summarized in Table 5.

The origin of the different extents of the Pt[d_{xz} + p_x] hybrid orbital contribution to the frontier orbitals can be rationalized by considering the molecular orbital pictures as the result of the {[$X(Me_3P)_2Pt]^{n+}$}−[5,12-diethynyltetracene dianion] interaction. Figure 10 shows the HOMOs and LUMOs (LUMO+2 for **9′**) of the model complexes and their corresponding compositions from the "frozen" $[X(Me_3P)_2Pt]^{n+}$ and 5,12-diethynyltetracene dianion fragments.

For the $[X(Me_3P)_2Pt]^{n+}$ fragments, mixing of the d_{xz} and p_x orbitals of the Pt ion and the π orbitals of the auxiliary ligand X gives rise to three hybrid orbitals {Pt[d_{xz} + p_x] + π(X)}, which are abbreviated as π(Pt) orbitals hereafter. These π(Pt) hybrid orbitals have π symmetry which are able to interact with the HOMO and HOMO-6 of the 5,12-diethynyltetracene dianion fragment to give the HOMO of the model complexes. The π(Pt) orbitals for the neutral complexes (**3′**−**6′**) are higher lying than those for the cationic complexes (**8′**−**10′**) by at least 4 eV because of the lower effective nuclear charge of the Pt ions in the neutral complexes. Therefore the π(Pt) orbitals in **3′**−**6′** have better energy matching with the HOMO and HOMO-6 of the 5,12-diethynyltetracene dianion fragment and thus contribute more to the HOMOs of the complexes than in the cases for **8′**−**10′**. The lower HOMO energies for **8′**−**10′** in comparison with those for **3′**−**6′** mainly arise from the higher nuclear charges of the $[X(Me_3P)_2Pt]^{n+}$ fragments in **8′**−**10′** in comparison to those in **3′**−**6′**. The LUMOs of the model complexes (LUMO+2 for **9′**) are mainly composed of the LUMO of the 5,12-diethynyltetracene dianion with some contribution from the LUMO+1. Again the lower LUMO energies for **8′**−**10′** (LUMO+2 for **9′**) in comparison with those for **3′**−**6′** mainly arise from the higher nuclear charges of the $[X(Me_3P)_2Pt]^{n+}$ fragments.

Electronic transitions for the model complexes were calculated using the TD-DFT method. Calculated vertical transition energies are summarized in Table 6. The calculated spectra (Supporting Information, Figures S1−S7) of the models are in good agreement with the experimental spectra: each of them exhibits a lowest-energy dipole-allowed electronic transition in the visible region (λ_{max} 588−617 nm) originating from one-electron excitation from the HOMO to the LUMO (or HOMO to LUMO+2 for **9′**). The absorption maxima obtained from the TD-DFT calculations is in the order L^{Si} (583 nm) ≈ **8′**−**10′** (582−596 nm) < **3′**−**6′** (606−617 nm), which parallels the trend observed experimentally. Figure 11 depicts the energy levels of the HOMOs and the LUMOs and the energies associated with the transition between these MOs for L^H, L^{Si}, and other model Pt complexes.

Figure 12 depicts the energies of the HOMOs and LUMOs of the model Pt complexes and L^{Si} relative to those in L^H, which can be used to illustrate the reason for the red shift in absorption and fluorescence from neutral to cationic complexes.

The plot shows that the HOMOs and LUMOs (LUMO+2 for **9′**) for **8′**−**10′** are substantially stabilized (ca. 3 eV) nearly solely by the inductive effect of the two doubly charged $[X(PMe_3)_2Pt]^{2+}$ units (metal perturbations to these orbitals are shown to be <5%; see Table 5 and Figure 10). Since the HOMOs and LUMOs (LUMO+2 for **9′**) are stabilized to nearly the same extent in these cationic complexes, their HOMO → LUMO transition energies (HOMO → LUMO+2 for **9′**) are close to that for L^H and L^{Si}. On the other hand, the HOMOs for **3′**−**6′** are destabilized to a greater extent (0.7−0.9 eV) than the LUMOs (0.6−0.7 eV), which is a result of stronger metal perturbation in the HOMOs (5−10%) than in the LUMOs (<5%). Thus, their HOMO → LUMO transition energies are red-shifted in comparison with those in **8′**−**10′**.

CONCLUSION

Traditionally, the electronic and spectroscopic properties of oligoacenes are varied by substitution of the H atoms of the rings with heteroatoms or functional groups. In this work, we demonstrated that the absorption and fluorescence of Pt_2 5,12-diethynyltetracenes are subject to the influence of auxiliary ligands which are not directly attached to the ring. Despite the wide range of electronic properties of the ligands examined in this study, according to the absorption and emission energies, the complexes can be classified into two groups: complexes with anionic π-donating ligands (**1**−**6**) and complexes with neutral ligands (**7**−**10**). The S_0 → S_1 transition associated with all these complexes are calculated to originate from HOMO → LUMO transitions (HOMO → LUMO+2 for **9**). For **7**−**10**, the contribution of these orbitals from the $[X(Me_3P)_2Pt]^{n+}$ fragments are minimal, as the π(Pt) hybrid orbitals on the $[X(Me_3P)_2Pt]^{n+}$ fragments are too low-lying to interact with the HOMO and LUMO of the 5,12-diethynyltetracene dianion fragment; thus, their HOMO → LUMO transition energies (HOMO to LUMO+2 for **9**) are close to that for the ligand L^{Si}. On the other hand, the {$[X(Me_3P)_2Pt]^{n+}$}−[5,12-diethynyltetracene dianion] interaction in **1**−**6** is apparent, and the

dx.doi.org/10.1021/om300904b | *Organometallics* 2013, 32, 1620−1629

HOMO of the 5,12-diethynyltetracene dianion fragment is perturbed to a greater extent by the π(Pt) hybrid orbitals on the $[X(Me_3P)_2Pt]^{n+}$ fragments, as they are closer to the HOMO of the 5,12-diethynyltetracene dianion fragment than the LUMO. Thus, the $S_0 \rightarrow S_1$ transition energies for **1**−**6** are red-shifted in comparison with those for **7**−**10**.

■ ASSOCIATED CONTENT

Supporting Information

CIF files, giving crystallographic data for **4**−**6**, **7**·$2CH_2Cl_2$, **8**·$0.5C_3H_6O$·H_2O, and **9**·$2CH_2Cl_2$, and Tables S1−S7 and Figures S1−S7, giving structural parameters of the optimized structures of the model complexes and their calculated absorption spectra, respectively. This material is available free of charge via the Internet at http://pubs.acs.org.

■ AUTHOR INFORMATION

Corresponding Author

*E-mail for J.H.K.Y.: chmyiphk@nus.edu.sg.

Notes

The authors declare no competing financial interest.

■ ACKNOWLEDGMENTS

We are grateful to Prof. Koh Lip Lin and Ms. Tan Geok Kheng for determining the X-ray structures. The Ministry of Education (R-143-000-429-112) of Singapore and the National University of Singapore are thanked for financial support. The computational work was supported by a grant from the Hong Kong Research Grants Council (Project No. CityU 103911).

■ REFERENCES

(1) (a) Ito, K.; Suzuki, T.; Sakamoto, Y.; Kubota, D.; Inoue, Y.; Sato, F.; Tokito, S. *Angew. Chem., Int. Ed.* **2003**, *42*, 1159. (b) Moon, H.; Zeis, R.; Borkent, E.-J.; Besnard, C.; Lovinger, A. J.; Siegrist, T.; Kloc, C.; Bao, Z. *J. Am. Chem. Soc.* **2004**, *126*, 15322. (c) Lin, C.-Y.; Wang, Y.-C.; Hsu, S.-J.; Lo, C.-F.; Diau, E. W.-G. *J. Phys. Chem. C* **2009**, *114*, 687. (d) Schon, J. H.; Kloc, C.; Bucher, E.; Batlogg, B. *Nature* **2000**, *403*, 408. (e) Odom, S. A.; Parkin, S. R.; Anthony, J. E. *Org. Lett.* **2003**, *5*, 4245. (f) Baluschev, S.; Yakutkin, V.; Miteva, T.; Avlasevich, Y.; Chernov, S.; Aleshchenkov, S.; Nelles, G.; Cheprakov, A.; Yasuda, A.; Müllen, K.; Wegner, G. *Angew. Chem., Int. Ed.* **2007**, *46*, 7693. (g) Griffith, O. L.; Anthony, J. E.; Jones, A. G.; Lichtenberger, D. L. *J. Am. Chem. Soc.* **2010**, *132*, 580.

(2) (a) Anthony, J. E. *Angew. Chem., Int. Ed.* **2008**, *47*, 452. (b) Muller, A. M.; Avlasevich, Y. S.; Schoeller, W. W.; Mullen, K.; Bardeen, C. J. *J. Am. Chem. Soc.* **2007**, *129*, 14240.

(3) (a) Anthony, J. E.; Brooks, J. S.; Eaton, D. L.; Parkin, S. R. *J. Am. Chem. Soc.* **2001**, *123*, 9482. (b) Anthony, J. E.; Eaton, D. L.; Parkin, S. R. *Org. Lett.* **2002**, *4*, 15. (c) Chen, J.; Subramanian, S.; Parkin, S. R.; Siegler, M.; Gallup, K.; Haughn, C.; Martin, D. C.; Anthony, J. E. *J. Mater. Chem.* **2008**, *18*, 1961. (d) Lehnherr, D.; Murray, A. H.; McDonald, R.; Ferguson, M. J.; Tykwinski, R. R. *Chem. Eur. J.* **2009**, *15*, 12580. (e) Lehnherr, D.; Murray, A. H.; McDonald, R.; Tykwinski, R. R. *Angew. Chem., Int. Ed.* **2010**, *49*, 6190.

(4) (a) Kaur, I.; Jia, W.; Kopreski, R. P.; Selvarasah, S.; Dokmeci, M. R.; Pramanik, C.; McGruer, N. E.; Miller, G. P. *J. Am. Chem. Soc.* **2008**, *130*, 16274. (b) Kaur, I.; Stein, N. N.; Kopreski, R. P.; Miller, G. P. *J. Am. Chem. Soc.* **2009**, *131*, 3424. (c) Barlier, V. S.; Schlenker, C. W.; Chin, S. W.; Thompson, M. E. *Chem. Commun.* **2011**, *47*, 3754. (d) Ono, K.; Yamaguchi, H.; Taga, K.; Saito, K.; Nishida, J.-i.; Yamashita, Y. *Org. Lett.* **2008**, *11*, 149. (e) Chen, Z.; Müller, P.; Swager, T. M. *Org. Lett.* **2005**, *8*, 273.

(5) (a) Khan, M. S.; Al-Mandhary, M. R. A.; Al-Suti, M. K.; Al-Battashi, F. R.; Al-Saadi, S.; Ahrens, B.; Bjernemose, J. K.; Mahon, M. F.; Raithby, P. R.; Younus, M.; Chawdhury, N.; Kohler, A.; Marseglia, E. A.; Tedesco, E.; Feeder, N.; Teat, S. J. *Dalton Trans.* **2004**, 2377. (b) Fox, M. A.; Le Guennic, B.; Roberts, R. L.; Brue, D. A.; Yufit, D. S.; Howard, J. A. K.; Manca, G.; Halet, J.-F.; Hartl, F.; Low, P. J. *J. Am. Chem. Soc.* **2011**, *133*, 18433. (c) Partyka, D. V.; Esswein, A. J.; Zeller, M.; Hunter, A. D.; Gray, T. G. *Organometallics* **2007**, *26*, 3279. (d) Gao, L.; Peay, M. A.; Partyka, D. V.; Updegraff, J. B.; Teets, T. S.; Esswein, A. J.; Zeller, M.; Hunter, A. D.; Gray, T. G. *Organometallics* **2009**, *28*, 5669. (e) Lee, H. B.; Sharp, P. R. *Organometallics* **2005**, *24*, 4875. (f) Wang, B.-Y.; Karikachery, A. R.; Li, Y.; Singh, A.; Lee, H. B.; Sun, W.; Sharp, P. R. *J. Am. Chem. Soc.* **2009**, *131*, 3150. (g) Murahashi, T.; Fujimoto, M.; Oka, M.-a.; Hashimoto, Y.; Uemura, T.; Tatsumi, Y.; Nakao, Y.; Ikeda, A.; Sakaki, S.; Kurosawa, H. *Science* **2006**, *313*, 1104. (h) Murahashi, T.; Takase, K.; Oka, M.-a.; Ogoshi, S. *J. Am. Chem. Soc.* **2011**, *133*, 14908.

(6) (a) Heng, W. Y.; Hu, J.; Yip, J. H. K. *Organometallics* **2007**, *26*, 6760. (b) Hu, J.; Lin, R.; Yip, J. H. K.; Wong, K.-Y.; Ma, D.-L.; Vittal, J. J. *Organometallics* **2007**, *26*, 6533. (c) Hu, J.; Yip, J. H. K.; Ma, D.-L.; Wong, K.-Y.; Chung, W.-H. *Organometallics* **2009**, *28*, 51. (d) Hu, J.; Xu, H.; Nguyen, M.-H.; Yip, J. H. K. *Inorg. Chem.* **2009**, *48*, 9684. (e) Hu, J.; Yip, J. H. K. *Organometallics* **2009**, *28*, 1093. (f) Wong, W.-Y.; Ho, C.-L. *Coord. Chem. Rev.* **2006**, *250*, 2627.

(7) Nguyen, M.-H.; Yip, J. H. K. *Organometallics* **2010**, *29*, 2422.

(8) Armarego, W. L. F.; Chai, C. L. L., *Purification of Laboratory Chemicals*, 5th ed.; Elsevier: Amsterdam, 2003.

(9) Karstens, T.; Kobs, K. *J. Phys. Chem.* **1980**, *84*, 1871.

(10) (a) *SMART & SAINT Software Reference Manuals, version 4.0*; Siemens Energy and Automation, Inc., Analytical Instrumentation: Madison, WI, 1996. (b) Sheldrick, G. M. *SADABS: Software for Empirical Absorption Correction*; University of Göttingen, Göttingen, Germany, 1996. (c) *SHELXTL Reference Manual, version 5.03.*; Siemens Energy and Automation, Inc., Analytical Instrumentation: Madison, WI, 1996.

(11) Becke, A. D. *J. Chem. Phys.* **1993**, *98*, 5648.

(12) Lee, C.; Yang, W.; Parr, R. G. *Phys. Rev. B* **1988**, *37*, 785.

(13) Andrae, D.; Häussermann, U.; Dolg, M. S., H.; Preuss, H. *Theor. Chim. Acta* **1990**, *77*, 123.

(14) (a) Hehre, W. J.; Ditchfield, R.; Pople, J. A. *J. Chem. Phys.* **1972**, *56*, 2257. (b) Hariharan, P. C.; Pople, J. A. *Theor. Chim. Acta* **1973**, *28*, 213. (c) Francl, M. M.; Petro, W. J.; Hehre, W. J.; Binkley, J. S.; Gordon, M. S.; DeFrees, D. J.; Pople, J. A. *J. Chem. Phys.* **1982**, *77*, 3654.

(15) (a) Krishnan, R.; Binkley, J. S.; Seeger, R.; Pople, J. A. *J. Chem. Phys.* **1980**, *72*, 650. (b) McLean, A. D.; Chandler, G. S. *J. Chem. Phys.* **1980**, *72*, 5639. (c) Blaudeau, J.-P.; McGrath, M. P.; Curtiss, L. A.; Radom, L. *J. Chem. Phys.* **1997**, *107*, 5016. (d) Curtiss, L. A.; McGrath, M. P.; Blaudeau, J. P.; Davis, N. E.; Binning, R. C.; Radom, L. *J. Chem. Phys.* **1995**, *103*, 6104.

(16) Frisch, M. J.; Trucks, G. W.; Schlegel, H. B., Scuseria, G. E., Robb, M. A.; Cheeseman, J. R.; Montgomery, J. A., Jr.; Vreven, T.; Kudin, K. N.; Burant, J. C.; Millam, J. M.; Iyengar, S. S.; Tomasi, J.; Barone, V.; Mennucci, B.; Cossi, M.; Scalmani, G.; Rega, N.; Petersson, G. A.; Nakatsuji, H.; Hada, M.; Ehara, M.; Toyota, K.; Fukuda, R.; Hasegawa, J.; Ishida, M.;Nakajima, T.;Honda, Y.; Kitao, O.; Nakai,H.; Klene, M.; Li, X.; Knox, J. E.; Hratchian, H. P.; Cross, J. B.; Bakken, V.; Adamo, C.; Jaramillo, J.; Gomperts, R.; Stratmann, R. E.; Yazyev, O.; Austin, A. J.; Cammi, R.; Pomelli, C.; Ochterski, J. W.; Ayala, P. Y.; Morokuma, K.; Voth,G. A.; Salvador, P.;Dannenberg, J. J.; Zakrzewski, V. G.; Dapprich, S.; Daniels, A. D.; Strain, M. C.; Farkas, O.; Malick, D. K.; Rabuck, A. D.; Raghavachari, K.; Foresman, J. B.;Ortiz, J. V.; Cui, Q.; Baboul, A. G.; Clifford, S.; Cioslowski, J.; Stefanov, B. B.; Liu, G.; Liashenko, A.; Piskorz, P.; Komaromi, I.; Martin, R. L.; Fox, D. J.; Keith, T.; Al-Laham, M. A.; Peng, C. Y.; Nanayakkara, A.; Challacombe, M.; Gill, P. M. W.; Johnson, B.; Chen, W.; Wong, M. W.; Gonzalez, C.; Pople, J. A. *Gaussian 03, revision D.01*; Gaussian, Inc., Wallingford, CT, 2004.

(17) Sonogashira, K.; Takahashi, S.; Hagihara, N. *Macromolecules* **1977**, *10*, 879.

(18) (a) Tao, C.-H.; Zhu, N.; Yam, V. W.-W. *Chem. Eur. J.* **2005**, *11*, 1647. (b) Ghosh, S.; Chakrabarty, R.; Mukherjee, P. S. *Inorg. Chem.*

2009, *48*, 549. (c) Liu, L.; Poon, S.-Y.; Wong, W.-Y. *J. Organomet. Chem.* **2005**, *690*, 5036. (d) Poon, S.-Y.; Wong, W.-Y.; Cheah, K.-W.; Shi, J.-X. *Chem. Eur. J.* **2006**, *12*, 2550. (e) Wong, W.-Y.; Wang, X.-Z.; He, Z.; Djurisic, A. B.; Yip, C.-T.; Cheung, K.-Y.; Wang, H.; Mak, C. S. K.; Chan, W.-K. *Nat. Mater.* **2007**, *6*, 521. (f) Zhou, G.; Wong, W.-Y.; Poon, S.-Y.; Ye, C.; Lin, Z. *Adv. Funct. Mater.* **2009**, *19*, 531. (g) Wong, W.-Y.; Liu, L.; Poon, S.-Y.; Choi, K.-H.; Cheah, K.-W.; Shi, J.-X. *Macromolecules* **2004**, *37*, 4496. (h) Wong, W.-Y.; Lu, G.-L.; Choi, K.-H.; Shi, J.-X. *Macromolecules* **2002**, *35*, 3506.

(19) (a) Johnson, C. A.; Haley, M. M.; Rather, E.; Han, F.; Weakley, T. J. R. *Organometallics* **2005**, *24*, 1161. (b) Arévalo, A.; Bernès, S.; García, J. J.; Maitlis, P. M. *Organometallics* **1999**, *18*, 1680. (c) Constable, E. C.; Housecroft, C. E.; Neuburger, M.; Schaffner, S.; Shardlow, E. J. *Dalton Trans.* **2005**, 234. (d) Crisp, M. G.; Tiekink, E. R. T.; Rendina, L. M. *Inorg. Chem.* **2003**, *42*, 1057. (e) Pilkington, M. J.; Slawin, A. M. Z.; Williams, D. J.; Woollins, J. D. *J. Chem. Soc., Dalton Trans.* **1992**, 2425.

(20) Birks, J. B. *Photophysics of Aromatic Molecules*; Wiley: London, 1970.

(21) Nguyen, M.-H.; Yip, J. H. K. *Organometallics* **2011**, *30*, 6383.

(22) (a) Steffen, A.; Tay, M. G.; Batsanov, A. S.; Howard, J. A. K.; Beeby, A.; Vuong, K. Q.; Sun, X.-Z.; George, M. W.; Marder, T. B. *Angew. Chem., Int. Ed.* **2010**, *49*, 2349. (b) Ma, C.; Chan, C. T.-L.; Kwok, W.-M.; Che, C.-M. *Chem. Sci.* **2012**, *3*, 1883.

(23) Ishida, H.; Tsubomura, H. *J. Photochem.* **1974**, *2*, 285.